E. Hay and M. W. Brown†*

Initiation and Early Growth of Fatigue Cracks from a Circumferential Notch Loaded in Torsion

REFERENCE Hay, E. and Brown, M. W., **Initiation and Early Growth of Fatigue Cracks from a Circumferential Notch Loaded in Torsion**, *The Behaviour of Short Fatigue Cracks*, EGF Pub. 1 (Edited by K. J. Miller and E. R. de los Rios) 1986, Mechanical Engineering Publications, London, pp. 309–321.

ABSTRACT Fatigue crack growth rates for notched specimens loaded in torsion are compared for various materials, temperatures and specimen sizes, using data from three different publications. It is demonstrated that the mode III stress intensity factor cannot provide a unifying parameter for crack propagation at different temperatures, but a reasonable correlation is obtained by using an elasto-plastic strain intensity factor that characterizes mode III deformation close to the crack tip. An upper bound equation is derived to give conservative estimates of crack growth rate, the strain intensity factor being derived from the ultimate shear stress of the material.

Notation

da/dN	Fatigue crack growth rate
G	Modulus of rigidity
ΔK_{III}	Stress intensity factor range (Mode III)
M_A	Maximum applied torque
M_L	Limit torque
r	Radius from specimen centre line
r_o	Specimen maximum radius
r_n	Specimen minimum radius (to crack tip)
r_p	Radius to edge of plastic zone
τ_y	Shear yield stress
τ_{ult}	Shear ultimate stress
Γ_{III}	Maximum strain intensity factor (Mode III)

Introduction

Under normal circumstances rotating shafts may be considered to transmit a constant torque, but frequently an oscillating component is superimposed on this constant torque and, under conditions of torsional resonance, such oscillations can cause yielding at stress concentrating features which can lead to the formation of fatigue cracks. An example of such a component is shown in Fig. 1, a compressor motor shaft of EN3A approximately 150 mm diameter.

* International Research and Development Co. Limited, Fossway, Newcastle upon Tyne NE6 2YD.
† University of Sheffield, Mechanical Engineering Department, Mappin Street, Sheffield S1 3JD.

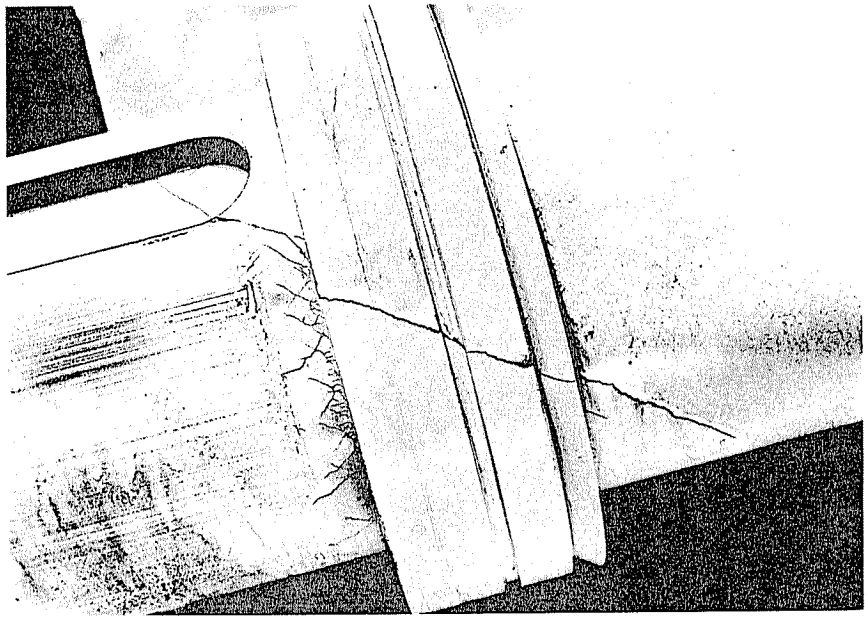

Fig 1 Cracking associated with an oil seal collar and keyway

Materials, specimen geometries, test conditions

Results of reversed torsion fatigue tests, carried out in air, from three sources are compared here. In each case the specimen was of circular cross-section with a circumferential vee-notch (Fig. 2). The sources and testing conditions were:

(a) from Brown, Hay, and Miller (**1**) on 1% Cr–Mo–V steel at ambient temperature and 565°C, specimen diameter 10 mm with a 1 mm deep notch;
(b) from Tschegg (**2**) on AISI 4340 steel at ambient temperature, specimen diameter 12.7 mm with a 0.631 mm deep notch;
(c) from Tschegg (**3**) on AISI 4340 steel at ambient temperature, specimen diameter 25.4 mm with a 1.06 mm deep notch;

Tables 1 and 2 show the chemical composition and mechanical properties of the materials considered.

Table 1 Chemical composition (wt %)

	C	*Mn*	*Ni*	*Cr*	*Mo*	*Si*	*p*	*S*	*Cu*	*V*	*Remainder*
1% Cr–Mo–V	0.24	0.64	0.21	1.02	0.57	0.29	0.016	0.01	—	0.29	Fe
AISI 4340	0.4	0.78	1.77	0.81	0.25	0.26	0.07	0.013	0.14	—	Fe

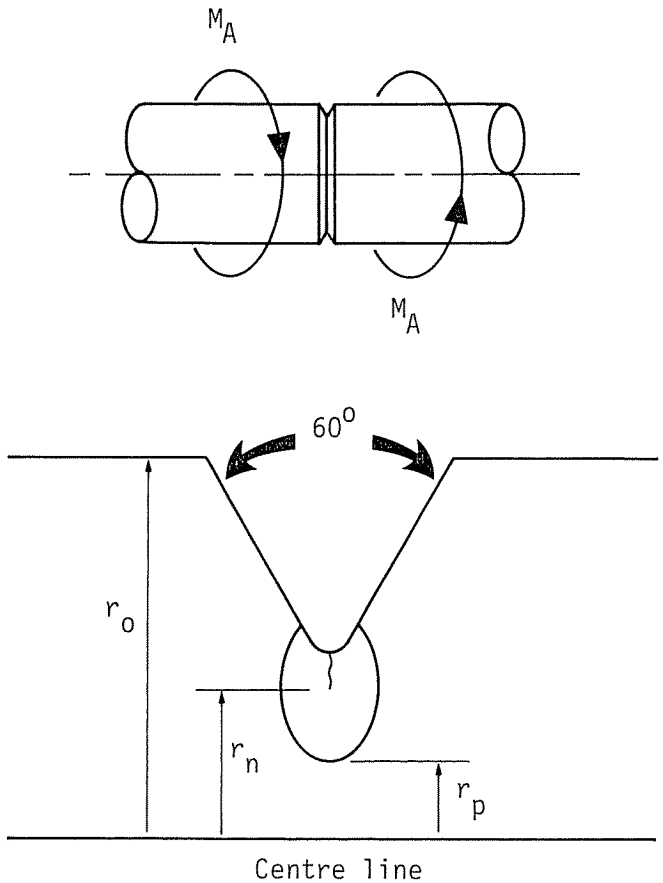

Fig 2 Specimen geometry

Table 2 Mechanical properties

	1% Cr–Mo–V		*AISI 4340*
	Room Temp.	*565°C*	*Room Temp.*
Ultimate tensile strength (MPa)	805	547	1076
Ultimate shear strength (MPa)	481	261	
Torsion yield strength (MPa)	336	198	552*

* For AISI 4340 Torsion Yield Strength was taken as $1/\sqrt{3}$ times the tensile yield strength.

In the cases compared here a small constant axial tension was applied to the specimen to minimize crack face rubbing and interference. The tests reported in (**1**) were conducted under constant angular deflection while those in (**2**) and (**3**) were conducted under constant quasi-apparent ΔK_{III} conditions, the applied torque being reduced as the fatigue crack depth increased. Fatigue crack depth was monitored in each case using the d.c. potential drop technique.

Fractography

After fatigue testing, a number of specimens were cooled in liquid nitrogen and broken under impact loading. Two distinct fracture surfaces were produced by different test conditions, which have been designated 'factory roof' (Fig. 3) and 'flat' (Fig. 4), in the 1% Cr–Mo–V steel.

The factory roof type of fracture surface was produced by the lower values of applied stress intensity range both at room and elevated temperatures. Under

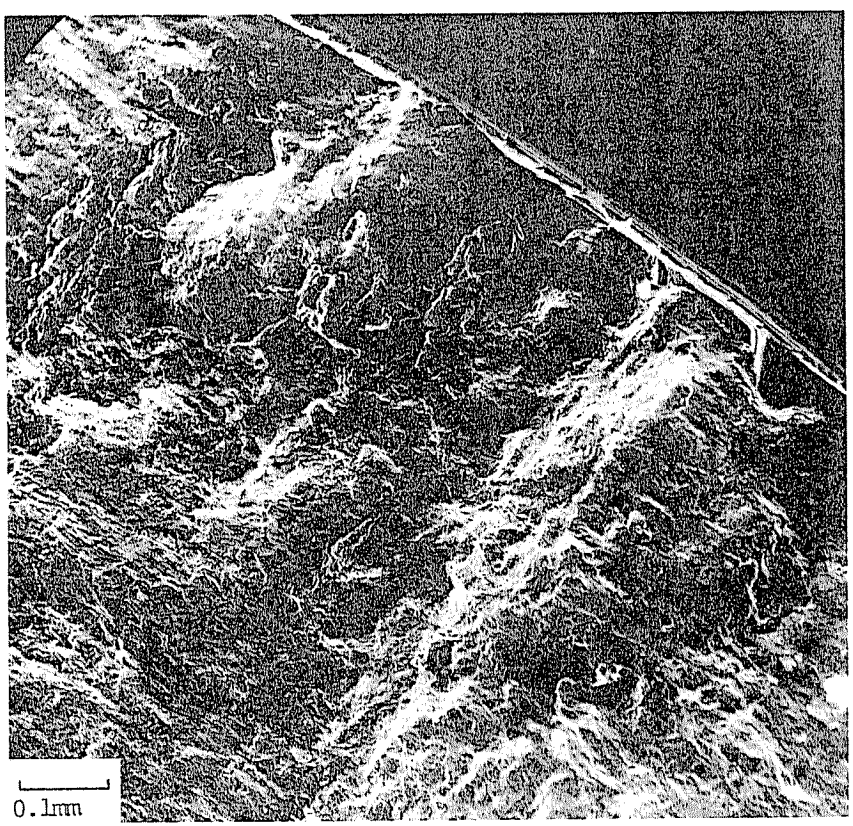

Fig 3 Factory roof fracture surface in 1% Cr–Mo–V steel at 20°C. Initial torque 34.8 Nm

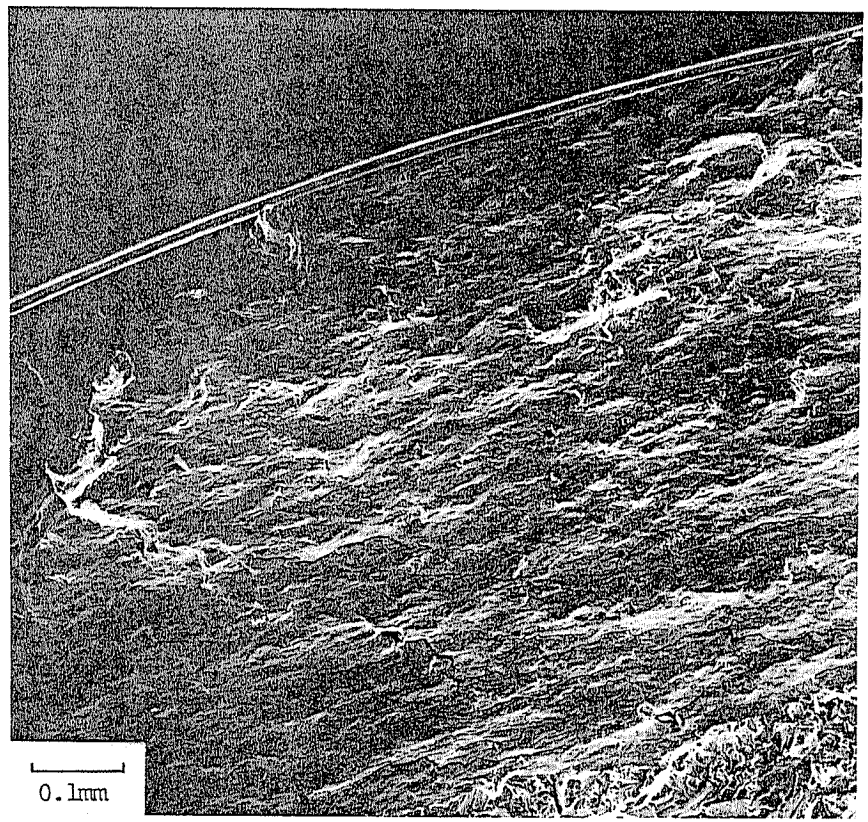

Fig 4 Flat fracture surface in 1% Cr–Mo–V steel at 20°C. Initial torque 60.1 Nm

constant angular deflection conditions (**1**), several cracks propagated by a mode I mechanism at approximately 45 degrees to the plane of the notch and linked up to give the serrated fracture surface; see also Fig. 1. The cracks propagated radially in these 45 degree planes until the applied stress intensity factor increased to a value where the mode of cracking changed to a mode III type, which gave a flat fracture surface. If the initial loading produced a high value of stress intensity factor range the crack initiated in mode III and a flat fracture surface was produced across the entire cross-section. The change-over in fracture mode occurred at a crack growth rate of 10 nm/cycle at room temperature and 100 nm/cycle at 565°C. The application of axial load did not affect the major features of the fracture surfaces, but did reduce the amount of surface rubbing. This was most evident on the flat fracture surfaces.

For AISI 4340 steel, tests were carried out under apparent constant stress intensity conditions, the applied torque being progressively reduced as the

cracks propagated. Fracture surfaces again showed flat faces at high stress intensity values and factory roof facets at low values of stress intensity factor. Where cracks were propagated to a depth of up to 4.5 mm in the range of ΔK_{III} 30 to 60 MPa$\sqrt{m}$ a change from an external flat to an internal section factory roof fracture surface was produced coincident with a reduction in crack growth rate, indicating that there was some crack face rubbing preventing the full effect of the applied loading being felt at the tip of the long crack. This change occurred at a crack depth which depended on the value of ΔK_{III}, but always in the region of a crack growth rate of 100 nm/cycle.

Fatigue crack growth behaviour

The present analysis has been confined to small cracks of depth less than 0.6 mm for the results from (**1**), and less than 1 mm for results from (**2**) and (**3**), since this corresponds to the greatest portion of fatigue lifetime. On a circumferential crack the axial force applied gave a mode I stress intensity factor of less than 3 MPa$\sqrt{m}$, but this force had a significant effect on crack growth behaviour, permitting maximum crack growth rates to be achieved by minimizing crack flank interference. In practical situations such high crack growth rates could be achieved by imposed bending stresses.

The fatigue crack growth rates, at room and elevated temperature, with an applied axial tension, are shown versus ΔK_{III} in Fig. 5. The results from different sources show agreement for the ambient temperature tests, but the results of tests carried out at 565°C show a different scatter band. Thus a single expression may not be used to describe fatigue crack growth behaviour in terms of ΔK_{III} at both temperatures.

The fatigue crack growth data of (**1**) were plotted against Γ_{III}, a plastic strain intensity factor based on the work of Walsh and MacKenzie (**4**) and Nayeb-Hashemi *et al.* (**5**)

$$\Gamma_{III} = \lim_{r \to r_n} \{\gamma(r_n - r)\}$$

$$= \frac{\tau_y}{G}\left(\frac{r_n}{r_p}\right)^2 (r_n - r_p) \qquad (1)$$

where r, r_p, and r_n are defined in Figure 2. Here, $(r_n - r_p)$ is the plastic zone size, which is given by (**5**)

$$\frac{r_p}{r_n} = 1 - qM^2 - M^4(1 - q - 1.5873(1 - M)^{1/3}) - 3.17(M^5 - M^6)$$

where

$$q = \frac{(16/9)\{(r_o/r_n) - 1\}}{1 + (64/9)\{(r_o/r_n) - 1\}}$$

and

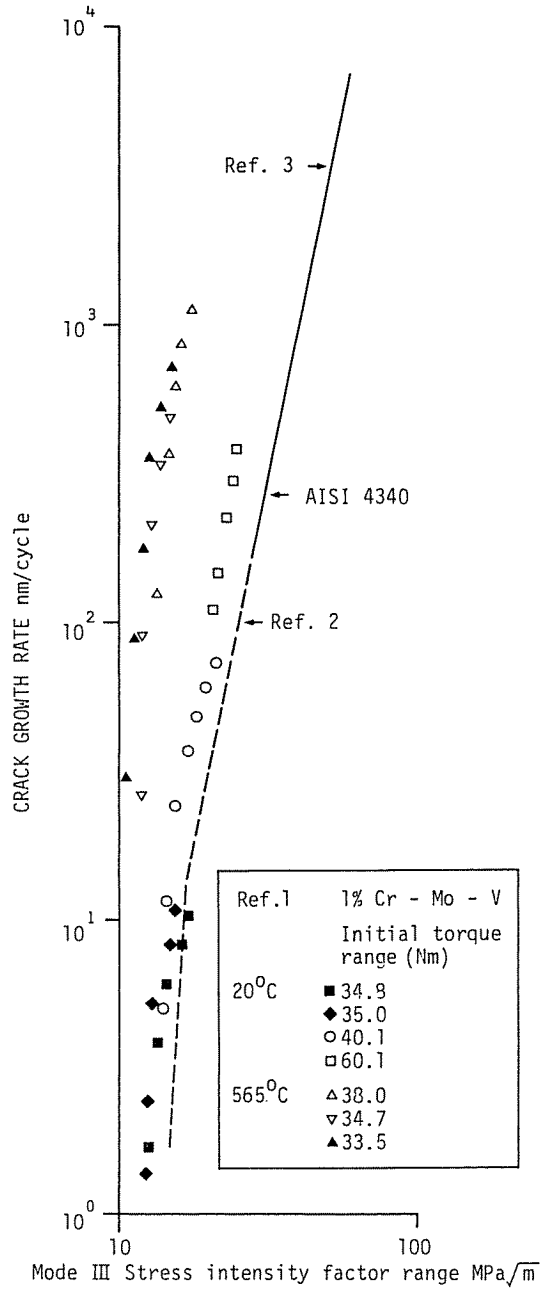

Fig 5 Crack growth rates versus stress intensity factor range

$$M = M_A/M_L$$

where M_A = maximum applied torque and M_L = limit torque = $(2/3)\pi\tau_y r_n^3$.

These equations assume elastic–perfectly plastic behaviour. To avoid the additional complications of strain hardening effects in the real material, the monotonic yield stress, τ_y, was replaced by the ultimate shear stress, τ_{ult}, of the material, since this gives a better estimate of cyclic flow stress. Comparison of the results at ambient and elevated temperature, Fig. 6, shows that there is no clear separation of the two sets of results, the curves from different tests falling into one band for the 1% Cr–Mo–V steel. The arrows in Fig. 6 indicate that the tests, carried out under constant angular deflection, produced increasing crack growth rates. The results from (**2**) and (**3**) were recalculated so that fatigue crack growth rates could be plotted as a function of Γ_{III}. A value for ultimate shear stress was used assuming that the ultimate shear stress was $1/\sqrt{3}$ of the value of the ultimate tensile stress. Figure 7 shows the fatigue crack growth rates versus Γ_{III} for these results on AISI 4340 steel. Here also there is no discernible distinction between the two sets of results due to a specimen size effect. The arrows in Fig. 7 show that the crack growth rates decreased under constant ΔK_{III} test conditions.

Discussion

Figure 8 shows the results of tests conducted under angular deflection control (increasing fatigue crack growth rates) and those of tests conducted under constant ΔK_{III} conditions (decreasing fatigue crack growth rates). No clear separation exists for the various conditions considered namely (a) two temperatures for one material, (b) two materials at one temperature, and (c) three specimen sizes. Thus the strain intensity factor gives a parameter which achieves a unification of results which is not possible using elastic stress intensity factors.

Figure 8 may be divided into three regions according to the type of fatigue cracking produced. At crack growth rate less than 10 nm/cycle, region A, the cracks form a factory roof type of surface; at crack growth rates greater than 100 nm/cycle, region C, flat fracture faces are produced; and between these, region B, is a transition region where a change occurs between factory roof and flat surface morphologies.

From Fig. 8 it is clear that some crack face interference effects are still present despite the application of axial tension, but an upper bound may be set from which a conservative estimate of early fatigue crack growth from a notch can be made. The extent of crack face interference, or crack closure, will be difficult to quantify since the actual morphology of individual fracture surfaces close to the crack tip will dictate both the relevant closure stress and the amount of crack face sliding subsequent to closure. Variation in closure conditions will be particularly great in the case of factory roof cracking, since the depth of individual 45 degree facets can vary widely from one crack to another. Thus the

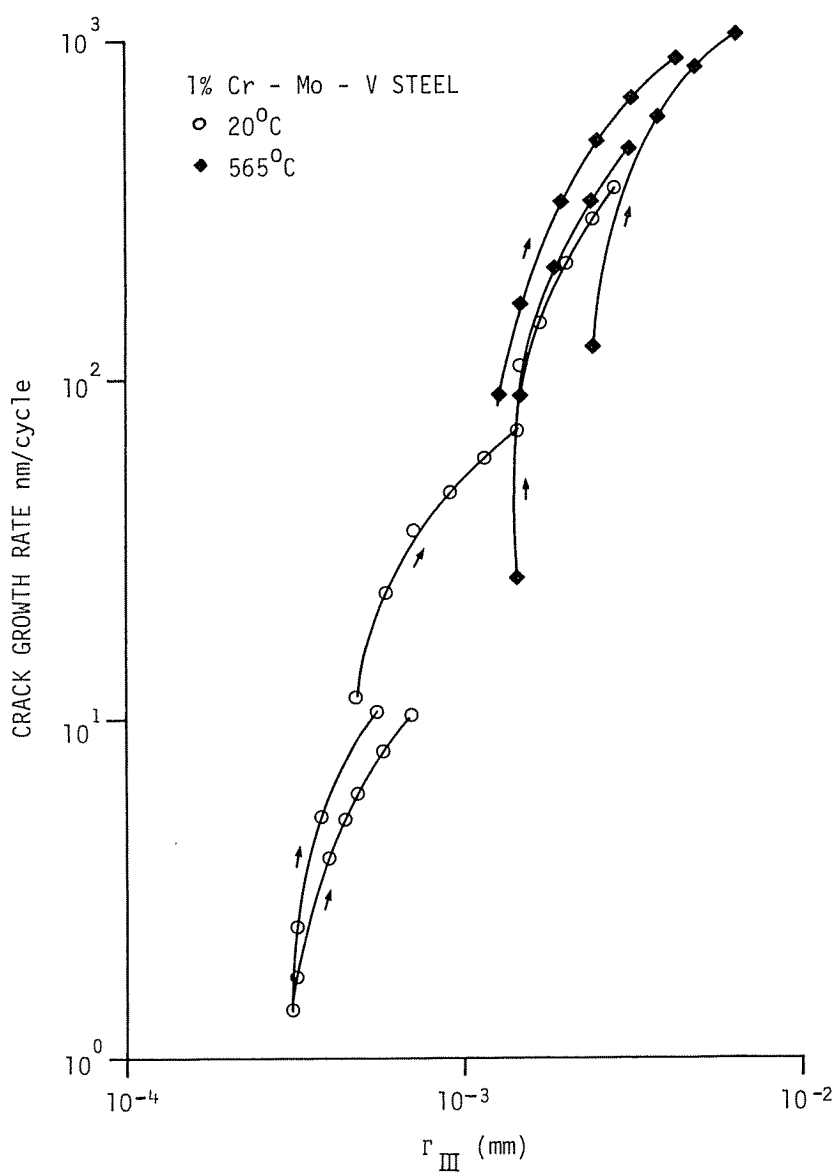

Fig 6 Crack growth rate versus maximum strain intensity for 1% Cr–Mo–V steel

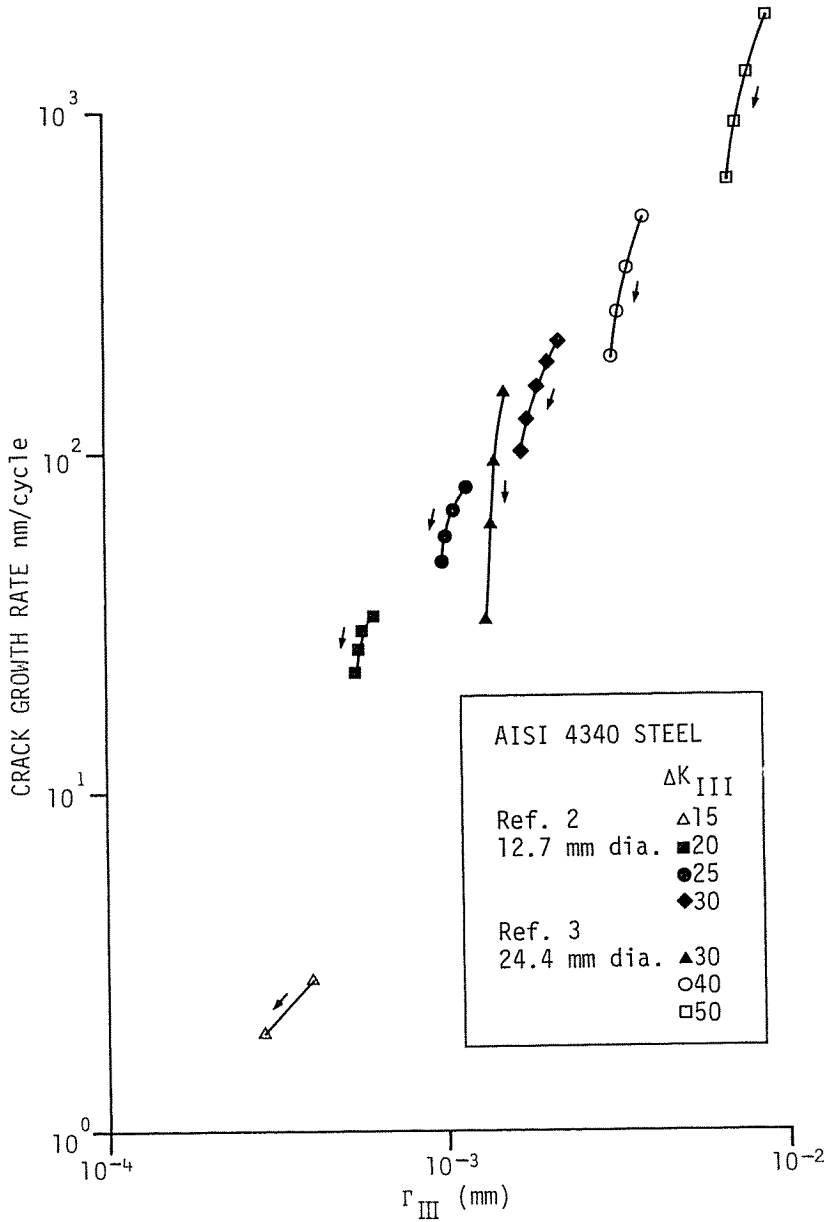

Fig 7 Crack growth rate versus maximum strain intensity factor for AISI 4340 steel (2)(3) where ΔK_{III} is given in MPa$\sqrt{m}$

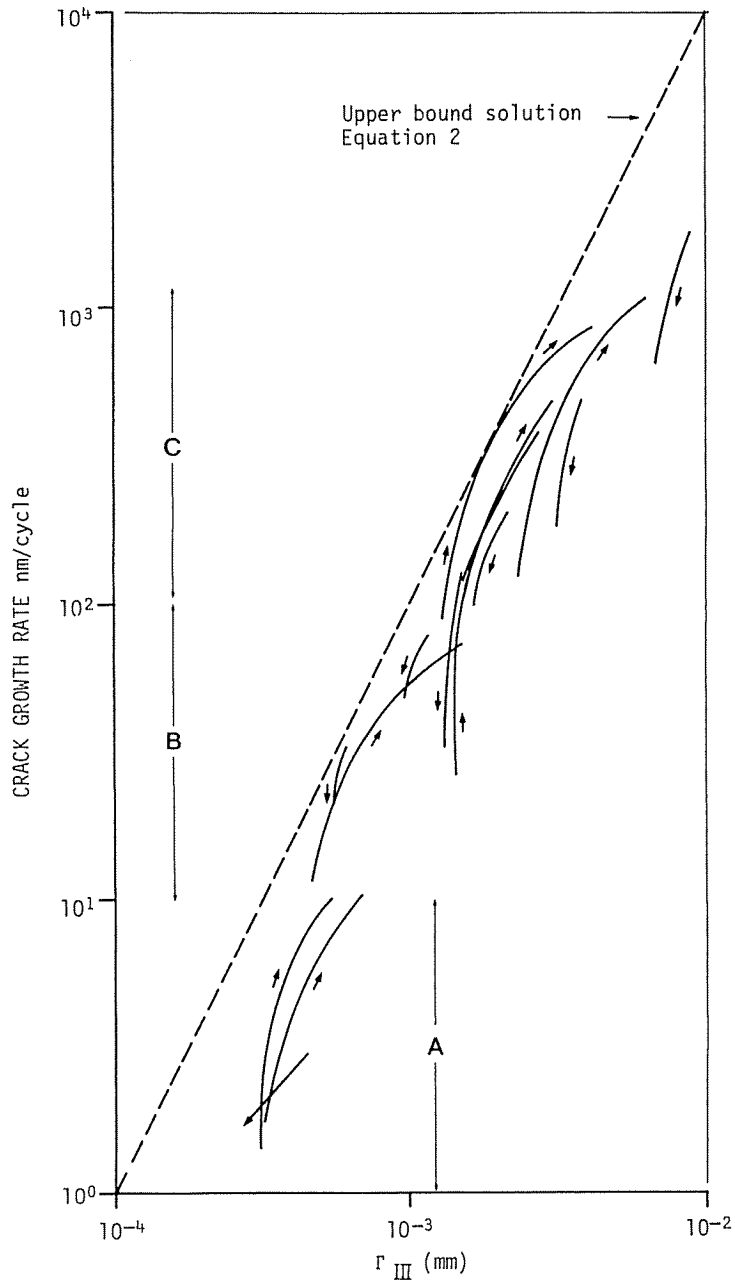

Fig 8 Crack growth rate versus maximum strain intensity factor for tests conducted under angular deflection control and constant stress intensity factor range

use of an upper bound solution which embraces closure effects, provides an expedient method of quantifying mode III crack propagation in components experiencing cyclic torsion.

The upper bound solution indicated in Fig. 8 may be described by

$$\frac{da}{dN} = 0.1\Gamma_{III}^2 \tag{2}$$

where da/dN is in μm/cycle and Γ_{III} is in μm.

This equation can only be used with the cyclic strain intensity factor amplitude, Γ_{III}, which itself is calculated from equation (1) using the ultimate shear stress as the cyclic flow stress, τ_y, and the applied torque amplitude, M_A. The curves in Fig. 8 suggests the possible presence of a threshold value for Γ_{III} in the region of 0.2 to 0.3 μm, below which equation (2) would not apply. However, the change to a mode I dominant type of cracking at low growth rates suggests that failure by mode I crack growth (see Fig. 1) can be expected, unless stresses are sufficiently low to keep below the mode I threshold (**1**). This apparent mode I threshold for factory roof fracture surfaces will also be highly susceptible to crack closure effects (**6**).

Conclusions

For circumferentially notched members loaded in reversed torsion, with a small axial tension applied, the following conclusions may be drawn.

(1) The stress intensity factor does not give a unifying parameter which will describe fatigue crack growth at different temperatures.
(2) The strain intensity factor (Γ_{III}) unifies mode III fatigue crack growth results from different materials, temperatures and specimen geometries.
(3) An upper bound equation may be used to give a conservative estimate of fatigue crack growth rates occurring above a threshold value of Γ_{III}.

Acknowledgements

The authors are indebted to E. K. Tschegg whose detailed experimental work has made the analysis possible. The authors are grateful to the Central Electricity Generating Board for provision of test material and for sponsorship of the project through a research fellowship and an SERC/CEGB Case Award.

References

(1) BROWN, M. W., HAY, E., and MILLER, K. J. (1985) Fatigue at notches subjected to reversed torsion and static axial loads, *Fatigue Fracture Engng Mater. Structures*, **8**, 243–258.
(2) TSCHEGG, E. K. (1983) Mode III and Mode I fatigue crack propagation behaviour under torsional loading, *J. Mater. Sci.* **18**, 1604–1614.
(3) TSCHEGG, E. K. (1982) A contribution to Mode III fatigue crack propagation, *Mater. Sci. Engng*, **54**, 127–136.
(4) WALSH, J. B. and MacKENZIE, A. C. (1959) Elastic–plastic torsion of a circumferentially notched round bar, *J. Mech. Phys Solids*, **7**, 247–257.

(5) NAYEB-HASHEMI, H., McCLINTOCK, F. A., and RITCHIE, R. O. (1982) Effect of friction and high torque on fatigue crack propagation in Mode III, *Met. Trans A*, **13A**, 2197–2204.
(6) TSCHEGG, E. K. (1983) The influence of the static I load mode and R ratio on Mode III fatigue crack growth behaviour in mild steel, *Mater. Sci. Engng*, **59**, 127–137.